X-ray Photoelectron Spectroscopy of Neutral and Electrochemically Doped Poly(*p*-phenylene vinylene)

Maria J. Obrzut† and Frank E. Karasz*

Department of Polymer Science and Engineering, University of Massachusetts, Amherst, Massachusetts 01003. *Received April 15, 1988*

ABSTRACT: The electronic structures of neutral and electrochemically doped poly(*p*-phenylene vinylene) (PPV) have been examined by X-ray photoelectron spectroscopy (XPS). The C(1s) core level spectra in the hexafluoroarsenate-doped PPV show component peak asymmetry and satellite positions which are sensitive to dopant content. The interpretation of the electronic structure has been assisted by theoretical studies of low molecular weight model compounds on the HAM/3 level. The features of the XPS valence-level spectra in the neutral polymer can be explained in terms of states derived from the tight binding model for conjugated chains by means of the VEH method. In the vicinity of the Fermi level the density of states is reduced by doping, but defect/hole states are not directly observed. The results further suggest that neither the detectable arsenic 4d orbitals nor the fluorine 2s orbitals contribute to the doped polymer valence band.

Introduction

Poly(*p*-phenylene vinylene) (PPV) belongs to a class of conjugated polymers which becomes electrically conducting upon the addition of electron donors or acceptors.[1] It has been shown that after exposure to oxidizing molecular dopants, the electrical conductivity of free standing PPV films increases by 12 orders of magnitude into the metallic regime.[2,3] Recently the mechanism of conductivity in nondegenerate conjugated polymers has been of particular interest because it has been suggested that bipolarons may be involved.[4] Although it is clear that the high conductivity is related to a charge transfer between the dopant and PPV, the detailed nature of this mechanism remains under discussion.

Thin films of PPV can be electrochemically cycled between the conducting and insulating states;[5] this provides the basis for the electrochemical characterization of PPV. The redox reaction involves oxidation of the delocalized π-electron system in the polymer backbone resulting in the formation of localized defects at 2.1 and 0.8 eV located within the 2.45 eV energy gap. On the other hand, the appearance of two doping related absorption bands in the PPV optical spectrum suggests polaron and bipolaron excitations. These were anticipated in the continuum electron–phonon model of *cis*-polyacetylene[7,8] as well as in numerical simulations for poly(*p*-phenylene).[9]

To complement the theoretical effort, in addition to optical spectroscopy, photoelectron spectroscopy also seems to be an attractive tool for studying conducting polymers. The chemical and electronic structure of doped polyacetylene has been examined by this technique[10,11] which has also been used in studies of polypyrrole systems.[12-14] In this paper the results of XPS core and valence level studies of neutral and electrochemically doped PPV are presented. The experimental data are discussed in conjunction with a theoretically calculated XPS spectrum, giving the energy band structure and density of states.

Experimental Section

I. Materials. Poly(*p*-phenylene vinylene) was obtained via the sulfonium salt precursor polymer.[2] Thin films cast from aqueous solutions of precursor polymer in an inert atmosphere were converted to PPV by heating at 10^{-4} Torr and 320 °C for 3 h. Platinum gauze (52 mesh, Fisher) was used as a film support in the measurements. Lithium foil (Aldrich, electrochemical grade) was used without further purification. Propylene carbonate (Burdick and Jackson Laboratories) was degassed under vacuum, and lithium hexafluoroarsenate (US Agrichemicals, electrochemical grade) was used as received. Doping of the PPV films (typically 0.1–0.2 μm thick) was accomplished by electrochemical oxidation using as electrolyte a solution of 1 M $LiAsF_6$ in propylene carbonate. The electrochemical redox cycle consists of an anodic wave with a current maximum at 3.85 V and a cathodic wave with a maximum at 3.8 V versus a Li/Li^+ reference electrode. Doped potentiostatic samples were washed in toluene and dried under vacuum. Samples and materials were handled in a drybox under argon.

II. Apparatus and Measurements. The potential, current, charge, and potential sweep rate during the electrochemical cycle were controlled by a Model 273 Princeton Applied Research potentiostat/galvanostat.

The photoelectron spectra were recorded at room temperature by using a Perkin-Elmer PHI 5000 LS ESCA system controlled by a Perkin-Elmer 7500 computer. The spectrometer was equipped with an Al $K\alpha_{1,2}$ monochromatized X-ray source providing 0.6 eV resolution. The energy calibration of the system was checked with Au and Ag standards using either Au $4f_{7/2}$ or Ag $3d_{5/2}$ lines at the Fermi edge. The fwhm (<0.6 eV) of the Ag $3d_{5/2}$ peak was measured following a subtraction of the background intensity linearly interpolated between the background intensities at binding energies 3 eV above and below the Ag $3d_{5/2}$ peak. Doped polymeric films were sufficiently conducting to prevent electrostatic charging; however, Au clusters deposited on the samples were used to check the zero binding energy scale. The electrostatic charging occurring for insulating samples was lowered by flooding the samples with thermal electrons and ensuring that variation of the flooding current resulted in uniform binding energy shifts of all signals. Binding energies for insulating samples are quoted relative to the hydrocarbon C(1s) peak at 284.6 eV.[15] For quantitative chemical analysis, the Perkin-Elmer (C(1s), F(1s), As(3d), and O(1s) atomic sensitivity factors (ASF) were used[15] which are based upon cross sections corrected for the kinetic energy dependence of the mean free path of the photoelectrons in the sample. The required ASF values were checked against the approximate peaks of $LiAsF_6$, poly(tetrafluoroethylene), and poly(methyl methacrylate) of known composition. Approximately 10^5 scans were collected in the valence spectrum region to obtain an acceptable signal-to-noise ratio.

III. Calculations. The HAM/3 molecular orbital program for the study of C(1s) core–hole ionization of low molecular weight analogues of PPV was obtained from ref 16. Atomic coordinates for the model molecules were taken from our earlier work.[6] For the model of the PPV backbone we consider only the planar aromatic trans conformation and its quinoid form with alternating single and double bonds lengths of 1.48 and 1.37 Å, respectively. Our version of HAM/3 is limited to a few members of row I elements, and computations for the arsenic salt were not possible. Since the properties of the doped polymeric system are not critical with respect to variations in dopant species, we replaced AsF_6^- with OH^- when examining the counterion bonding effect by including it in the SCF procedure.[17]

The electronic states and their densities in the valence region were computed on the basis of a tight binding model (VEH)[4] for an idealized one dimensional lattice of *trans*-PPV. The method employs linear combinations of Bloch adapted Gaussian orbitals

† On leave from Institute of Physics, Cracow Polytechnic, Poland.

0024-9297/89/2222-0458$01.50/0

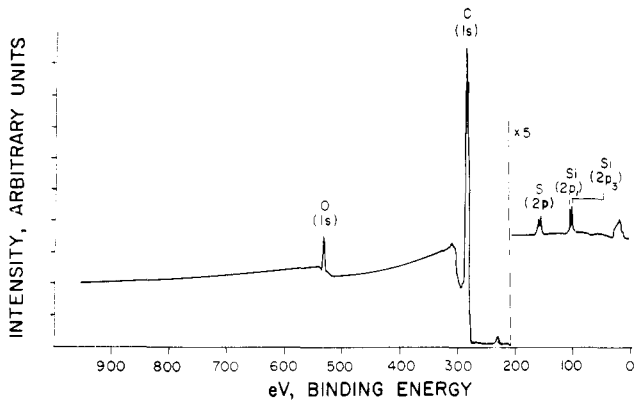

Figure 1. XPS survey spectrum of PPV.

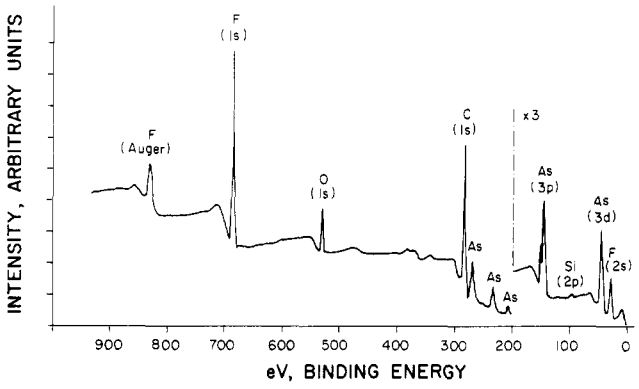

Figure 2. XPS survey spectrum of PPV electrochemically doped with AsF_6^-.

of double-ζ quality for the p and s states. The potential is constructed from a superposition of atomic potentials of the PPV unit cell generated from self-consistent Hartree–Fock charge densities. The potential matrix elements were calculated in momentum space to convergence. All overlap integrals of a magnitude lower than 10^{-8} were neglected.

The density of states histogram was calculated from VEH eigenvalues as described in ref 18. The algorithm consisted of continuous integration throughout the small intervals located at each k_{x_i} point for which a diagonalization was performed.

The theoretical XPS valence spectra were calculated on the basis of the density of states accounting for the known photoionization cross-sections[19] and for the inherent resolution limitation of the spectrometer.[18]

Results and Discussion

I. Core Level Spectra. ESCA survey spectra of the neutral and AsF_6^- electrochemically doped PPV films, measured for binding energies of 1000 through 0 eV are shown in Figures 1 and 2, respectively. The spectrum of neutral PPV shows a C(1s) peak at 284.6 eV and a O(1s) peak at 532.0 eV. There are also relatively low-intensity peaks associated with S(2s) at 229 eV, S(2p) at 165 eV, and Si(2s) at 153 eV, Si(2p) at 102 eV, respectively. The presence of residual Si and S stems from side reactions during the polymer synthesis.

From these results elemental analysis of the top 40 Å of the film surface yielded 96.6% C and 2.5% O; S and Si are below 1%. Oxygen was present in the surface layer even though the samples were prepared and handled in a high-purity inert atmosphere with only a short exposure to air during insertion into the spectrometer.

The ESCA spectrum of doped PPV displays additional bands characteristic of arsenic As($3p_1$) at 148 eV, As($3p_3$) at 144 eV, As($3d_5$) at 44 eV, fluorine F(1s) at 686 eV, and F(2s) at 30.6 eV as well as those of neutral PPV. The atomic composition near the surface for doped PPV is 3.4% O, 76.3% C, 7.9% As, and 11.3% F. The fluorine-/arsenic and carbon/arsenic ratios in the samples were constant during storage at room temperature at pressures below 10^{-8} Torr over a period of several days and remained essentially constant after exposure to air; the oxygen content increased a few percent. We note that samples of electrochemically doped conducting PPV exhibited a more stable optical absorption and electrical conductivity than those doped from the gas phase.

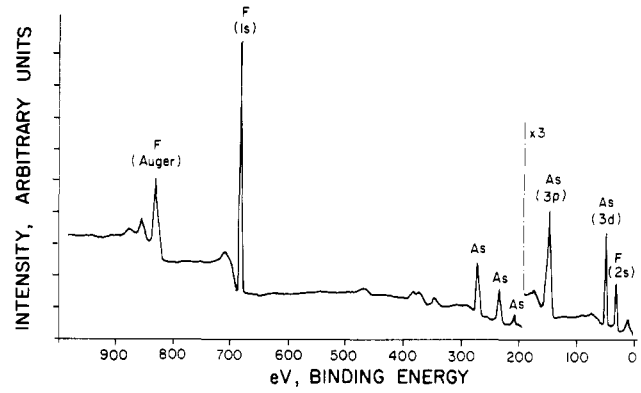

Figure 3. XPS survey spectrum of $LiAsF_6$.

The ESCA spectra of $LiAsF_6$ are shown in Figure 3, where a close similarity in the As and F signals to those observed in doped PPV is apparent, confirming our expectation that the dopant is present as the AsF_6^- anion rather than as a product of its degradation. A similar deduction can be made from the atomic composition and is consistent with the electrochemical cycle.

Thus a model of the electrochemical doping process in which electrons are extracted from the PPV conjugated system offers a simple chemical model for the doped material. This corresponds to a radical cation diffused over eight polymer units or a spinless dication diffused over four polymer units stabilized by AsF_6^- counteranion(s).[5]

In Figure 4 the C(1s) high-resolution spectra for neutral and doped PPV are presented. The dopant influence on the PPV electronic structure appears as high binding energy components of the C(1s) peak with intensities depending on the dopant content. A satellite structure is seen at about 6.5 eV above the main peak. Its possible correspondence to a shake-up process in which simultaneous core–electron excitations and π–π^* transitions occur is discussed in section I.A. A shape analogous to that observed here for the C(1s) spectra is often observed for oxygen derivatives of hydrocarbons with the higher binding energy component assigned to the carbon–oxygen bond.[20,21] In o-bis(phenol), for instance, the spacing between the components was found to be about 1.8 eV;[22] in carbonyl-, carboxyl-, or ether-containing organic compounds the spacing varies between 1.2 and 1.8 eV depending on the charge withdrawal from the oxygen-bonded carbon.[22,23] Thus the effect here can be attributed to a local nonequivalence of electron densities on the carbon atoms and was also detected in electrochemically oxidized polymers. However, even in polypyrrole, which is probably the best understood system, the origin of these components of the C(1s) and N(1s) peaks is still a subject of controversy. The effect was first attributed to oxygen[24] and then later to the dopant.[25] A localized displacement in the charge distribution caused by a counteranion has not been recently questioned[12-14] although no splitting in the (polypyrrole)$^+BF_4^-$ C(1s) and N(1s) peaks had been detected earlier; then it was concluded that uniform charge extraction from the polymeric matrix occurred.[26]

In the PPV system we cannot rule out the interference of oxygen since it is found in higher concentrations after

Table I
Gaussian Components of C(1s) Spectra from Figure 4

sample		area %	position (eV)	fwhm[a] (eV)
neutral PPV	C_a	82	284.6	1.1
	C_b	18	285.5	2.2
PPV doped 5% As	C_a	79	284.6	1.0
	C_b	4	285.4	0.5
	C_c	17	286.5	1.3
PPV doped 7% As	C_a	65	284.6	1.1
	C_b	6	285.4	0.6
	C_c	29	286.5	1.6

[a] fwhm = full width at half-maximum.

doping. It is noteworthy however that the only concentrations of elements consistent with the charge involved during the electrochemical cycle are those of As and F.

The spectra presented in this paper contain 10^4 to 10^5 scans for a typical sample size, and the statistical quality ensures that the experimental resolution is in the instrumental range. Therefore the multimodal character of the spectra in Figure 4 can be attributed to the sample itself. The dashed curves in Figure 4 show Gaussian/Lorenzian components deconvoluted from experimental results using the Fletcher–Powell method[27] when the χ-square values corresponded to about 92–95% goodness of fit. The fitting results are summarized in Table I.

A. C(1s) Ionization in Neutral PPV. The C(1s) spectrum of neutral PPV (Figure 4a) consist of two components at 284.6 eV (80% area) and at 285.5 eV (20% area). The interpretation of this spectrum was assisted by theoretical studies on low molecular weight systems. We have chosen *p,p'*-vinylenebis(stilbene) (DSV) (Figure 5) as the low molecular weight model for the PPV backbone. This in practice approaches the computational limits of the MO methods though we believe this model is appropriate since a core ionization process is strongly localized. Even in this extended conjugated system the nonuniform electron distribution is visible in Figure 5 where for example the electron population is lower on C_3. A fraction of similar centers is then expected to contribute to the higher binding energy component in Figure 4a as a part of C_b. The predicted energy of the C(1s) photoelectron peaks for the C_2 (286.0 eV), C_3 (287.0 eV), and C_4 (286.1 eV) carbons (Table II) seems to be consistent with the above picture; the components correspond to the nonuniform electron population of the carbon atoms within the PPV conjugated electronic system.

Although the calculated positions of the C(1s) peaks in DSV are somewhat different from those observed in PPV, due to oversimplification of the model, the 1 eV spacing between the values calculated for the C_3 and C_2, C_4 atoms is satisfactory. The remaining question however is how the shake-up process contributes to the C(1s) spectrum. The 2.5% oxygen detected on the surface of PPV film may also affect the spectrum. The shake-up process leads to states in which one (core) electron is ionized and another

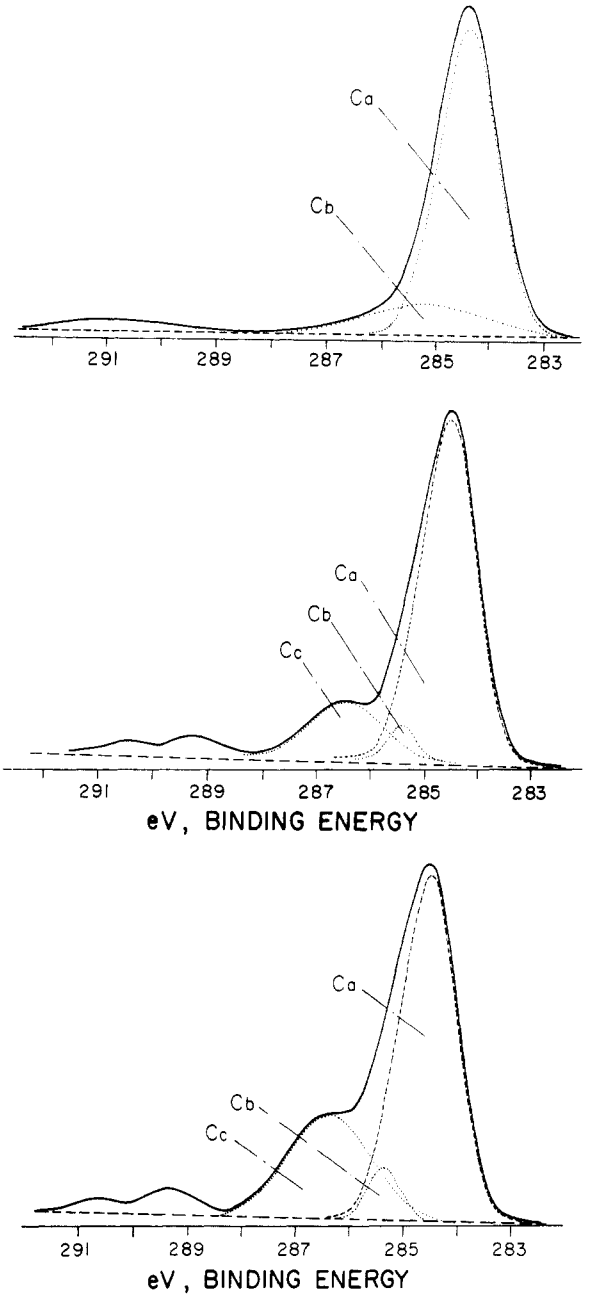

Figure 4. Carbon C(1s) spectrum of (a) undoped, (b) and (c) AsF_6^- doped PPV.

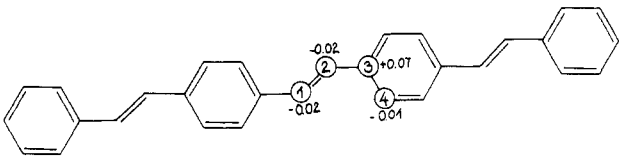

Figure 5. Representation of *p,p'-trans*-vinylenebis(stilbene) (DSV).

Table II
HAM/3 C(1s) Core-Hole Excitation Energies (eV) and Charge on Ionized Center

	carbon atom from which 1s electron was removed (Figure 5)					
	C_2		C_3		C_4	
model compound	core–hole	electron pop. in ionized center	core–hole	electron pop. in ionized center	core–hole	electron pop. in ionized center
DSV[a]	286.0	0.2553	287.0	0.2598	286.1	0.2572
DSV–oxygen complex (R = 2.5 Å)[a]	285.4	0.2547	285.0	0.2531	285.6	0.2540
DSV^+ valence cation[b]	288.2	0.2632	289.1	0.2675	288.3	0.2633
DSV^+–OH^- (R = 2.5 Å)[b]	285.6	0.2558	288.4	0.2663	285.9	0.2581

[a] Aromatic transplanar structure. [b] Quinoid transplanar structure.

(valence) electron is excited. We have approximated the energies for only the two main states: the two excited doublets which can be formed from the $\pi-\pi^*$ excitation in the presence of an $(N-1)$-electron, one-spin core–hole doublet state. An outline of the selected theoretical methods and their limitations is given elsewhere.[28,29]

The model compound is the DSV^+ ion with the core–hole localized on C_2. The influence of the core–hole on the valence states is simulated by employing HAM/3 methodology which has been shown to account for two electron processes.[28] In particular, the HAM/3 equivalent core–hole approach satisfactorily approximates core–valence Coulomb integrals by modifying the effective nuclear charge of the center to be ionized and accounts for the average energy of the partly relaxed core–hole configuration, E^{av}, directly.

Within our approximation the energy of the singlet coupled doublet $^2E^1(k)$ and triplet coupled doublet $^2E^3(k)$ are given as follows[29]

$$^2E^1(k) = E^{av} + {}^3/_2K_{ij} + {}^1/_2K_{jk} - {}^1/_2K_{ik}$$

$$^2E^3(k) = E^{av} - {}^1/_2K_{ij} + {}^3/_2K_{jk} + {}^1/_2K_{ik}$$

where K_{ij} is the valence–valence exchange integral evaluated in the neutral system. The K_{jk} and K_{ik} core–valence exchange integrals were evaluated as in the case of the completely localized core–hole: $K_{jk} = 1.2cj^2$ and $K_{ik} = 1.2c_i^2$ where c_i and c_j are the corresponding LCAO coefficients. The average excitation energy E^{av} refers to the partially relaxed configuration of the ion as is mentioned above. The calculated results show that relative to neutral DSV, the one-electron eigenvalues are reduced in the presence of the core–hole. The downward shift is substantial for the valence levels where the HOMO–LUMO energy gap decreases by about 2 eV, in accordance with the modification of the molecular orbitals. In response to the creation of a primary hole, the rearrangement of valence orbitals is such that about 75% of the core–hole charge is neutralized. Table III shows that core–hole ionization of the DSV C_2 atom yields several shakeup states of energies 1.7–4.0 eV above the C(1s) peak. It is seen that these results can be attributed to satellite structures at 291 eV in Figure 4a rather than to the 285.5 eV C_b component seen there. In contrast, the calculated energies of C(1s) ionization for the DSV–oxygen complex (Table II) are separated by only about 0.5 eV. Therefore, it is clear that the oxygen contamination can contribute to the C_b component and can result in the observed tail in the experimental peak.

B. C(1s) Ionization in Doped PPV. The C_c component at 286.5 eV (Table I) contributes to the C(1s) peak of doped PPV (Figure 4b,c) in addition to those of the C_a and C_b components. This is apparently a dopant-related feature with a maximum intensity at 1.9 eV above the C_a maximum and depending on the electrochemical balance. In comparison to the results discussed for the neutral system, we consider this result to be a manifestation of core ionization of the carbon atom in a highly oxidized state.

A simple model of dopant-like charge extraction, calculated with the HAM/3 method, can be constructed using the DSV^+ valence cation for which the core–hole ionization energy is calculated. It is seen in Table II that the calculated core–hole ionization energies for the DSV^+ which has one valence electron removed from $24a_u$ π orbital are in the range 288–289 eV which is inconsistent with the experimental data. This discrepancy between the calculated spectrum and experiment can be rationalized by noting the counterion stabilizing effect on the charge displacement in the oxidized conjugated system. The

Table III
Low-Lying Energies (eV) of Shake-Up Satellites $^2E^1_{i,j}$ and $^2E^3_{i,j}$ Calculated on the Basis of HAM/3 Electronic Properties of DSV and DSV^+(1s) Core-Hole Localized on Carbon C_2[a]

property			DSV	DSV^+(1s)
energy level E	symmetry	character	(eV)	(eV)
E_{j+2}	b_g	π^*	−2.289	−5.044
E_{j+1}	a_u	π^*	−3.029	−5.561
E_j	b_g	π^*	−3.621	−7.303
E_i	a_u	π	−5.910	−8.425
E_{i-1}	b_g	π	−6.384	−8.774
E_{i-8}	a_u	π	−8.111	−10.906
$^1B_u(\pi-\pi^*)$ singlet			2.597	1.571
$^3B_u(\pi-\pi^*)$ triplet			1.980	0.672
K_{ij}			0.3085	
$K_{i-1,j+1}$			0.3378	
$K_{i,j+2}$			0.3177	
$K_{i-8,j}$			0.2167	
$K_{i,k}$			3.0×10^{-3}	
$K_{i-1,k}$			0.0411	
$K_{i-8,k}$			0.0438	
$K_{j,k}$			0.2157	
$K_{j+1,k}$			7.7×10^{-3}	
$K_{j+2,k}$			0.0927	
$^2E^1_{i,j}$			1.7	
$^2E^1_{i-1,j+1}$			3.7	
$^2E^1_{i,j+2}$			3.9	
$^2E^1_{i-8,j}$			4.0	
$^2E^3_{i,j}$			1.3	
$^2E^3_{i-1,j+1}$			3.1	
$^2E^3_{i,j+2}$			3.4	
$^2E^3_{i-8,j}$			3.8	

[a] i refers to the $24a_u$ highest occupied molecular orbital (HOMO). j refers to the $24b_g$ lowest unoccupied molecular orbital (LUMO). k refers to 1s atomic level. The symmetry nomenclature is taken from the C_{2h} symmetry point group.

electrostatic polarization of dopant related centers should not be far different from those in the neutral system, since there is only 1.6 eV displacement between the C_c and C_a components. Comparison of the calculated results with experiment for the neutral system suggests a charge density on the PPV carbon with a core–hole only about 0.25 electron less due to compensation by the conjugated π-valence electrons. A corresponding value for $PPV^+AsF_6^-$ can be estimated similarly as low, as are the results calculated for DSV^+. Therefore the inadequacy of the results for the free DSV^+ valence ion is seen to improve after including the counterion in the computational scheme to yield a model electronic system more in accordance with the experimental system. The results in Table II show that the DSV^+ valence ion with an OH^- counterion 2.5 Å above the C_1,C_2 double bond (Figure 5) is a useful approximation reflecting the properties of doped PPV observed by core level XPS.

The calculated 285.6 eV C_2(1s) and 288.4 eV C_3(1s) ionization energy for the DSV ionic complex (Table II) is close to that of the experimentally observed spectrum in Figure 4b,c. In the presence of our artificial counterion, the rearrangement of valence orbitals in response to the creation of a core–hole neutralizes about 74% of the core–hole charge. Furthermore, counterion bonding with DSV^+ in that fixed position has been identified as a source of stabilization, yielding nonnegligible perturbations of the intramolecular properties of interest. Thus in the doped material, the effective field of the surrounding charges is of considerable importance. Even the simplifications inherent in the model structure of the DSV^+OH^- ionic complex has been shown to affect the electronic structure of DSV in the manner observed for doped PPV.

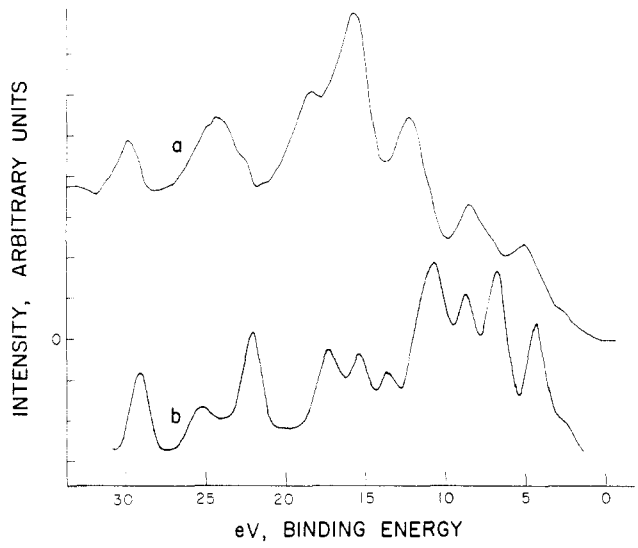

Figure 6. XPS valence spectrum of PPV: (a) experimental, referenced to the Fermi level of a standard with a work function of 3.9 eV; (b) calculated, for agreement with experiment the calculated spectrum was shifted by 1.2 eV toward higher binding energies.

Thus it is clear that counterion coupling to the ground and vibrationally excited intramolecular charge-transfer states effectively screens localized charge defects in the polymeric matrix. It should be emphasized, however, that due to uncertainties in the PPV^+ cation–counterion separation and the microscopic details of the pairing scheme within the doped quinoid and neutral aromatic sites, discussion in greater detail must be rather speculative.

In parts b and c of Figure 4 dopant-related satellite structures are seen at about 290 eV, which is nearly 2 eV lower in the binding energy scale if compared to the neutral system. In relation to Figure 4a the satellite structures have a higher intensity presumably corresponding to the deformation of valence molecular orbitals of the polymer matrix in the polar medium. Therefore in contrast to the neutral system, in doped PPV the π–π^* configuration has a symmetry which can interact with the primary hole configuration expressed by nonnegligible CI matrix elements.

II. Valence Level Spectra. The XPS valence spectrum of PPV is shown in Figure 6a. It consists of several relatively narrow photoionization peaks beginning at 3 eV.

We consider the experimental PPV XPS valence spectra as a manifestation of a condensed state effect, resulting in a lifting of the degeneracy and broadening of the XPS bands and causing the appearance of new low-energy bands characteristic of ordered systems of molecular sites.

Parts a and b of Figure 7 show the VEH one-dimensional energy band structure and density of states arising from four π and fifteen σ doubly occupied molecular orbitals in the *p*-phenylene vinylene unit cell, for which geometrical parameters were determined from electron diffraction on highly oriented films.[32] From an orbital analysis of the band eigenvectors, it is seen that the valence and conduction bands in the vicinity of the Fermi edge are due to the π overlap of the $2p_z$ orbitals of ethylene and the two connected aromatic carbons. The conduction and valence band widths are each nearly 1.5 eV along the chain direction, much less than in case of polyacetylene.[30]

The band gap of about 2.3 eV is consistent with the transparency of the material in the optical range. It is about 0.2 eV below the experimental absorption edge and differs from the value determined from the photoconduction threshold. We note however that the band gap

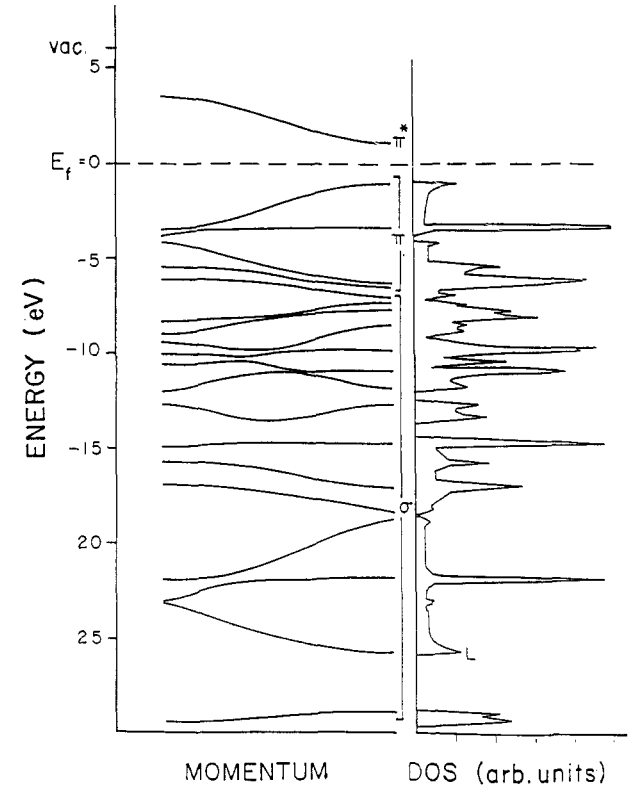

Figure 7. VEH energy band structure (a) and density of states (b) for stereoregular PPV chain.

of about 2.5 eV, in good agreement with the electronic absorption edge, is predicted when the geometry calculated for the stilbene molecule by the MNDO method[31,33] is applied to the *p*-phenylene vinylene unit cell. A number of additional calculations with a range of deviations from a uniform 1.397 Å C–C aromatic bond length to the weakly alternating carbon–carbon double-bonded 1.37 Å and carbon–carbon single-bonded 1.43 Å, and to quinoid bond lengths in the PPV repeat unit, yield an altered structure for the uppermost energy bands and appreciably lower the band gap.

In a *trans*-PPV single chain, there are always an even number of electrons per half cell translation and the Fermi level lies between the π valence and π^* conducting bands regardless of the bond lengths. Figure 7b shows the density of states calculated at 21 points in the irreducible part of the Brillouin zone which was used to calculate the XPS valence spectra shown in Figure 6b. The overall agreement between the theoretical predictions and experiment is satisfactory. Thus the photoelectrons detected between 3 and 7 eV in Figure 6a are attributable to the upper valence states arising from the first four π-character bands. The remaining 2s and $2p_{x,y}$ valence orbitals of carbon in an sp^2 hybridization result in bands below −7 eV (see Figure 7) which are formed from the overlap of σ bonds. The calculated photoelectron spectra based on σ states also provide a satisfactory agreement with experiment. We note that the density of states near the top of the valence band and the bottom of the conducting band is quite small. The calculated effective mass tensor element in the k_x direction of about $1.2m_e$ together with the 2.5 eV bandgap qualifies PPV as an insulating material ($\rho = 10^{16}$ Ω cm at 303 K) which excludes significant dark conductivity without modification. The latter is accomplished by doping which is assumed to transform the insulating lattice into a metal-like structure. The XPS valence spectrum of doped PPV is shown in Figure 8. The photoelectron peaks have reduced intensity, but the main feature close

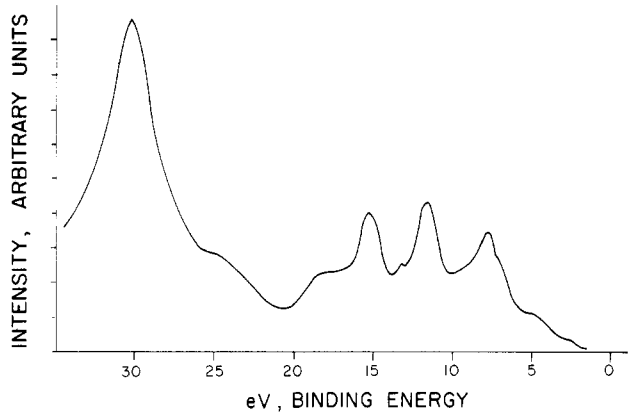

Figure 8. XPS valence spectrum of doped PPV.

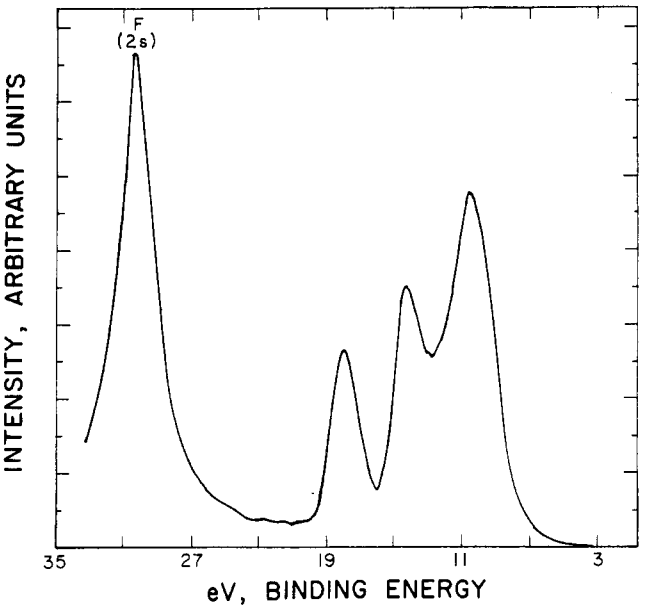

Figure 9. XPS valence spectrum of $LiAsF_6$.

to the Fermi level is similar to that of the neutral polymer lattice. No significant density of states can be seen by XPS in the vicinity of the Fermi energy after doping, which is the condition found in metals and metal-like organic charge-transfer complexes. Since the lowest clearly observable XPS feature in Figure 8 is a peak at 3 eV, the $PPV^+AsF_6^-$ valence band does not appear to be "metallic". The valence orbitals of the AsF_6^- counterion contribute to the valence level XPS spectrum of the $PPV^+AsF_6^-$ ionic complex with a binding energy above 10 eV. The core F(2s) is seen at about 30.5 eV, and other characteristics for AsF_6^- single hole state spectra shown in Figure 9 appear to be present also in the valence spectra of doped PPV, implying that the counterion–polymeric cation coupling is limited to localized defects.

Conclusion

In summary, we have studied the electronic structure of neutral and electrochemically doped poly(*p*-phenylene vinylene) by XPS spectroscopy. The core level C(1s) spectra for neutral PPV consist of narrow peaks characteristic of aromatic hydrocarbons. In the valence region the XPS spectra show an influence attributed to the condensed polymeric phase. With use of the VEH method, we have calculated the energy band structure and density of states for the PPV chain in the limit of a one-dimensional tight-binding model. Calculated XPS valence level spectra have been found to be essentialy consistent with experiment. Therefore the electronic structure observed up to 12 eV from the Fermi edge can be assigned to extended molecular states resulting from overlapping π and σ orbitals in the PPV conjugated chain. In comparison, in the doped polymer, XPS peaks close to the Fermi level are similar to those of the neutral polymer matrix. The observed hole states are more consistent with a disordered molecular solid than a one-dimensional metal. The atomic composition of the doped material is consistent with an electrochemical cycle in which charge is extracted from the polymer film attached to the electrode surface during oxidation. This process leads to the formation of the ionic complex $PPV^+AsF_6^-$, where the counteranion content is determined by the charge taken up in the electrochemical oxidation. The formation of the ionic complex and its electrochemical decomposition is reversible. When the electrochemical balance is restored and the charge extracted during oxidation is returned in the reduction step, the electronic structure of neutral PPV is restored. However, additional results imply that the pairing scheme between the localized polymeric cation site and the counteranion is not limited only to coulombic interaction.

The XPS C(1s) core level spectra of doped PPV indicate that positive charge is nonuniformly distributed over the polymeric matrix. The electron density is reduced on some carbon atom centers resulting in a dopant-related component structure displaced by 1.6 eV toward higher binding energies from the C(1s) peak. Several MO calculations for low molecular weight analogues of the PPV backbone with counteranion simulated perturbations in their valence orbitals suggest that counteranion coupling involves rearrangement of polymer and counteranion orbitals to yield an energetically favorable structure for the localized defects.

Acknowledgment. We are indebted to Dr. L. Salvetti, Jr., and the Physical Electronics Division of Perkin Elmer Corp. for assistance with the XPS experiments. We wish to thank Dr. J. L. Bredas and Professor J. M. Andre who provided a version of the VEH computer program. All calculations were performed on the CDC Cyber CY870 at the University of Massachusetts Computing Center. This work was supported by AFOSR Grant 84 0033.

Registry No. PPV, 26009-24-5; DSV, 64496-23-7; DSV^+, 117306-62-4; DSV^+OH^-, 117306-63-5; C, 7440-44-0; AsF_6^-, 16973-45-8; $LiAsF_6$, 29935-35-1.

References and Notes

(1) Hayes, W. *Contemp. Phys.* **1985**, *26*, 421.
(2) Gagnon, D. R.; Capistran, J. D.; Karasz, F. E.; Lenz, R. W.; Antoun, S. *Polymer* **1987**, *28*, 567.
(3) Murase, I.; Ohnishi, T.; Noguchi, T.; Hirooka, M.; Murakami, S. *Mol. Cryst. Liq. Cryst.* **1985**, *118*, 333.
(4) Bredas, J. L.; Themans, B.; Andre, J. M. *Phys. Rev. B: Condens. Matter* **1983**, *27*, 7827.
(5) Obrzut, J.; Karasz, F. E. *J. Chem. Phys.* **1987**, *87*, 6178.
(6) Obrzut, J.; Karasz, F. E. *J. Chem. Phys.* **1987**, *87*, 2349.
(7) Brazovskii, S. A.; Kirova, N. N. *Zh. Eksp. Teor. Fiz.* **1981**, *33*, 6.
(8) Fesser, K.; Bishop, A. R.; Campbell, D. K. *Phys. Rev. B: Condens. Matter* **1983**, *27*, 4804.
(9) Bredas, J. L.; Chance, R. R.; Silbey, R. *Phys. Rev. B: Condens. Matter* **1982**, *26*, 5843.
(10) Salaneck, W. R.; Thomas, H. R.; Bigelow, R. W.; Duke, C. B.; Plummer, E. W.; Heeger, A. J.; MacDiarmid, A. G. *J. Chem. Phys.* **1980**, *72*, 3674.
(11) Ikemoto, I.; Cao, Y.; Yamada, M.; Kuroda, H.; Hirada, I.; Shirakawa, M.; Ikeda, S. *Bull. Chem. Soc. Jpn.* **1982**, *55*, 721.
(12) Pfluger, P.; Street, G. B. *J. Chem. Phys.* **1984**, *80*, 544.
(13) Skotheim, T. A.; Florit, M. I.; Melo, A.; O'Grady, W. E. *Phys. Rev. B: Condens. Matter* **1984**, *30*, 4846.
(14) Eaves, J. G.; Munro, H. S.; Darker, D. *Polym. Commun.* **1987**, *28*, 38.
(15) Wagner, C. D.; Riggs, W. M.; Davis, L. E.; Moulder, J. F.; Muilenberg, G. E. *Handbook of X-ray Photoelectron Spec-*

troscopy; Perkin-Elmer Co. Physical Electronics Division: Minneapolis, MN, 1979.
(16) *Quantum Chemistry Program Exchange*; *No. 393.*
(17) Freund, H. J.; Bigelow, R. W. *Chem. Phys.* **1981**, *55*, 407.
(18) Delhalle, J.; Dehalle, S. *Int. J. Quantum Chem.* **1979**, *11*, 349.
(19) Delhalle, J.; Delhalle, S.; Andre, J. M. *Chem. Phys. Lett.* **1975**, *34*, 430.
(20) Thomas, H. R.; O'Malley, J. J. *Macromolecules* **1981**, *14*, 1316.
(21) Gardella, J. A., Jr.; Ferguson, S. A.; Chin, R. L. *Appl. Spectrosc.* **1986**, *40*, 244.
(22) Ahmed, A.; Adnot, A.; Kaliaguine, S. *J. Appl. Polym. Sci.* **1987**, *34*, 359.
(23) Kodama, D. M.; Kuramoto, K.; Carino, I. *J. Appl. Polym. Sci.* **1987**, *34*, 1889.
(24) Pfluger, P.; Krounbi, M.; Street, G. B. *J. Chem. Phys.* **1983**, *78*, 3212.
(25) Pfluger, P.; Gubler, U. M.; Street, G. B. *Solid State Commun.* **1984**, *49*, 911.
(26) Salaneck, W. R.; Erlandsson, R.; Prejza, J.; Lundström, J.; Inganäs, O. *Synth. Met.* **1983**, *5*, 125.
(27) Fletcher, R.; Powell, M. J. D. *Comput. J.* **1963**, 163.
(28) Lindholm, E.; Asbrink, L. *J. Electron Spectrosc. Related Phenom.* **1980**, *18*, 121.
(29) Bigelow, R. W.; Weagley, R. J.; Freund, H. J. *J. Electron Spectrosc. Relat. Phenom.* **1982**, *28*, 149.
(30) Chien, J. C. W. *Polyacetylene Chemistry, Physics and Materials Science*; Academic: New York, 1984.
(31) *Quantum Chemistry Program Exchange*; *No. 438.*
(32) Granier, T.; Thomas, E. L.; Gagnon, D. R.; Karasz, F. E. *J. Polym. Sci., Polym. Phys. Ed.* **1986**, *24*, 2793.
(33) *Quantum Chemistry Program Exchange*; *No. 379.*

Theoretical Equation of State: Thermal Expansivity, Compressibility, and the Tait Relation

R. K. Jain

Physics Department, Rajdhani College, University of Delhi, New Delhi 110015, India

Robert Simha*

Department of Macromolecular Science, Case Western Reserve University, Cleveland, Ohio 44118. *Received April 27, 1988; Revised Manuscript Received June 9, 1988*

ABSTRACT: Exact scaled expressions for the thermal expansivity α and the isothermal compressibility β are derived as functions of temperature and pressure. In the frame of the hole theory, α at atmospheric pressure has been frequently obtained as the derivative of an approximation to the exact volume–temperature function. Differences are seen, and an improved approximation is now extracted from the rigorous expression, which reduces the previous temperature dependence of α. Summaries of PVT measurements at elevated pressures and comparisons with theory are frequently presented in terms of the Tait equation. We derive formal expressions for the quantities C and B and observe variations of the "constant" C with pressure and temperature and a dependence of the temperature function B on pressure. These variations, even if numerically small in certain ranges of temperature and pressure, are significant for a computation of β or of bulk moduli. Accurate approximations to the theoretical C and B functions over specified ranges of the scaled variables are given. When substituted into the Tait expression for β, the results are numerically consistent with the analytical equations. They are computationally convenient and are recommended for the discussion of compressibilities and bulk moduli. The exact scaled expressions remain valid for multiconstituent systems.

Introduction

In recent times explicit equations of state (PVT), with emphasis on chain-molecular fluids, have been developed by a series of authors.[1-5] Moreover, comparisons between these theories in numerical[6-8] or analytical terms[9] have been presented.

Numerous studies of single-constituent and multiconstituent melts, the latter either as physical mixtures[10] or as copolymers,[11,12] have served to illustrate the quantitative success of the hole theory developed in ref 5 (SS). The configurational thermodynamic functions appear in scaled form, and the combination of experimental and scaled theoretical PVT surfaces then yields the scaling pressure P^*, temperature T^*, and volume V^* as characteristic *constants* of the particular system. This, of course, implies an adequate representation of the experimental data by the theoretical expressions.

The purpose of this paper is not the comparison of SS with other theories, sufficiently clarified by other authors, nor, for that matter, the relation to experiment, already explored extensively. However, two aspects merit further attention in the frame of the SS theory. Both have a bearing on the numerical procedures used in the evaluation of experimental data in terms of theory. Both involve temperature and volume derivatives. Besides the intrinsic interest in these functions, they play a role in the evaluation of the scaling parameters. Two coupled equations, one of these in trancendental form, involve the reduced variables of state and the vacancy fraction. A numerical approximation to the scaled volume–temperature function at zero reduced pressure has been most frequently employed to obtain the characteristic volume and temperature parameters. This has obvious implications for the theoretical prediction of thermal expansivities. Second, experimental data at elevated pressures have frequently been expressed and then employed in terms of the empirical Tait relation to test theories. An interpretation of this equation based on our theory remains to be investigated.

In what follows we obtain first exact expressions for the thermal expansivity as a function of temperature and pressure. Second, the functional dependencies of the Tait parameters are derived. The results of these computations are compared with previous results in terms of thermal expansivity and isothermal compressibility. No explicit experimental results are involved, and a scaled representation of all equations will be sufficient.

Recapitulation of Basic Equations

The reduced equation of state is[5]

$$\tilde{P}\tilde{V}/\tilde{T} = (1 - Q)^{-1} + (2y/\tilde{T})(A\Phi - B)\Phi \qquad (1)$$

with $Q = 2^{-1/3}y(y\tilde{V})^{-1/3}$, $\Phi = (y\tilde{V})^{-2}$, $A = 1.011$, and $B = 1.2045$. The vacancy fraction $1 - y$ for an s-mer satisfies the minimum condition on the free energy, viz.

0024-9297/89/2222-0464$01.50/0